Experiences of image-domain least-squares migration for quantitative interpretation

Maud Cavalca, Robin P. Fletcher and Robert Bloor, Schlumberger

This paper was prepared for presentation during the 16th International Congress of the Brazilian Geophysical Society held in Rio de Janeiro, Brazil, 19-22 August 2019.

Least-squares migration can help reduce non-geological amplitude variations caused by uneven illumination. Herein, we apply least-squares migration in the image domain to recover acoustic or elastic properties. Dip-dependent illumination and wavelet stretch effects are captured using point spread functions and mitigated through inversion in the image domain. We show how this approach, also referred to as depth-domain inversion, can efficiently account for illumination variations induced by different geological and acquisition settings, leading to higher-resolution and more reliable earth property estimates. We also show how the approach can be used to reconcile seismic vintages associated with different acquisition geometries for time-lapse analysis.

Introduction

Rarely do seismic experiments illuminate the subsurface in a uniform manner. In complex environments, the acquisition geometry limitation, coupled with the overburden complexity can lead to severe dip- and space-dependent illumination variations at the reservoir levels. If not accounted for, these non-geological variations can distort the amplitudes of the associated depth-migrated images and compromise the earth property estimates derived through conventional amplitude inversion.

Least-squares migration offers a way to account for variable illumination and recover amplitudes that are more representative of the underlying geology. By iteratively reducing the seismic experiment imprint (source wavelet, acquisition layout and overburden complexity), least-squares migration can significantly improve the resolution and amplitude fidelity of the images we are working with, making them closer to the true reflectivity.

Herein, we apply least-squares migration in the image domain. This type of approach, implemented, for instance, using point spread functions (PSFs), constitutes a viable alternative to more conventional schemes defined in the data domain (Fletcher et al., 2016) and is becoming increasingly popular due to its relative cost-effectiveness. Designing the least-squares migration problem in the image domain is also beneficial in terms of quality control of the inversion process. Because data, models, and inversion residuals are all defined in the same (geological) domain, data and model constraints are easily defined and residuals can be directly interpreted in terms of the level of confidence we have in the inverted models. This also makes local inversion straightforward.

Moreover, image-domain least-squares migration is readily parameterized and constrained in terms of earth properties (Fletcher et al., 2012), offering a way to estimate earth properties from the depth-migrated images through one single inversion in the depth domain. This process is referred to as depth-domain inversion.

In this paper, we share experiences of depth-domain inversion to recover acoustic and elastic properties from depth-migrated images generated in different geological environments and with different acquisition settings. We also use the approach for time-lapse analysis of non-repeatable seismic surveys.

Method

The least-squares migration/inversion framework regards the migrated image as the result of applying a linear modelling/migration operator, or blurring operator, to the subsurface reflectivity. This operator is a measure of resolution and illumination that reflects the limitations of the seismic experiment (acquisition and imaging system). Image-domain least-squares migration consists of deblurring the image, i.e., removing the effects of this operator from the image.

We approximate the blurring operator through its impulse responses or PSFs, computed through modelling and migration for a set of diffractor points in the subsurface and interpolated between these points. Deblurring is achieved through optimization by seeking the reflectivity model that, when convolved with the PSFs, best matches the migrated image. Moreover, by expressing the reflectivity as the result of applying a (possibly non-linear) reflectivity operator to the earth properties, the inversion problem is parameterized and constrained in terms of acoustic or elastic earth properties. This approach is referred to as depth-domain inversion (Fletcher et al., 2012).

The success of this approach at deconvolving and compensating for variable illumination largely depends on the ability of each PSF to capture these variations upon modelling and migration within the seismic experiment. An adequate source wavelet and propagator must be employed, which may mean working with disconnected modelling and migration algorithms to account for the effects of the various migration optimization features while preserving accurate modelling (Cavalca et al., 2016), accounting for residual absorption effects (Cavalca et al., 2015), or handling source/receiver ghost effects (Caprioli et al., 2014). Nevertheless, because some of the

propagation effects cannot be modelled (e.g., elastic effects…), inconsistencies between the PSFs and the seismic image(s) are unavoidable. Calibrating the PSFs using the reflectivity calculated from well logs helps alleviate these residual mismatches, particularly in the vicinity of the wells.

Inversion examples in salt environments

Illumination variations induced by the presence of salt structures can create massive amplitude variations in the associated subsalt images. If not accounted for, these non-geological amplitude variations are translated into erroneous earth property variations.

The first example is taken from a subsalt area in the Green Canyon of the Gulf of Mexico (Letki et al., 2015a). Amplitude dimming was observed in the central part of the reverse time migration (RTM) image due to a drop in illumination in this area. Conventional time-domain seismic inversion relying on a 1D wavelet estimated at the well mapped these low amplitudes into low acoustic impedances. The process inherently assumed that the amplitude variations were reflective of the geology. On the other hand, by capturing the spatially-variant illumination effects in the PSFs (3D wavelets), depth-domain inversion accounted for the illumination drop and helped recover more continuous and reliable acoustic impedance in this area (Figure 1).

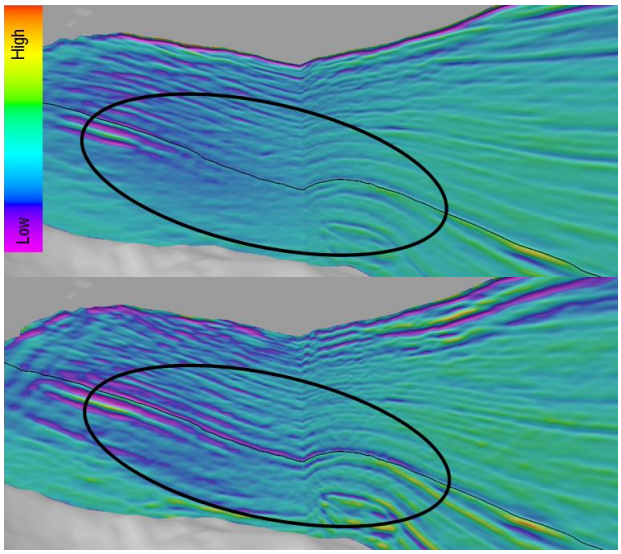

Figure 1 - *Gulf of Mexico subsalt RTM example: Acoustic impedance volume derived with conventional time-domain inversion (top), and depth-domain inversion (bottom). [From Letki et al., 2015a]*

This technique was applied in other complex salt environments, including the subsalt area of the Brazilian Santos Basin (Letki et al., 2015b). In this case, the benefits of depth-domain inversion over time-domain inversion were particularly visible in areas of large structural dip variations, such as in the layered salt. The PSFs successfully captured the dip-dependent illumination effects, leading to higher-fidelity acoustic impedance estimates in areas originally affected by strong dip-dependent wavelet effects (Figure 2).

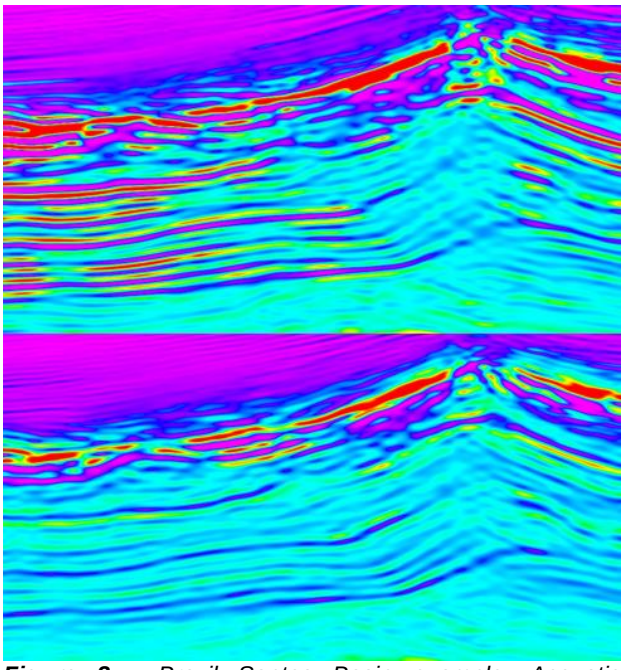

Figure 2 - *Brazil Santos Basin example. Acoustic impedance volume derived with conventional time-domain inversion (top), and depth-domain inversion (bottom). The acoustic impedance lateral variations visible in the result from conventional time-domain inversion are a direct mapping of the amplitude variations caused by dip-dependent illumination effects (present in the RTM image). These non-geological variations are significantly reduced through depth-domain inversion, leading to more balanced acoustic impedance layers. [From Letki et al., 2015b]*

Working in salt environments requires special care. Energetic salt events often dominate the inversion, slowing down (or even jeopardizing) convergence to an acceptable solution. This can be prevented by using spatially variant weights that down-weight these energetic events. Because, data (image) and model (earth properties) are defined in the same domain, the design of data inversion weights and constraints is facilitated.

Moreover, deriving accurate results close to the salt boundaries (or close to any sharp velocity discontinuity) may require employing more sophisticated PSF interpolators as well as techniques to handle the multi-scattering artifacts present in the PSFs close to the boundaries (Fletcher et al., 2018). These techniques were used in the following example from the Mississippi Canyon in the Gulf of Mexico (Leon et al., 2018). The target prospect in this area was characterized by several relatively thin sand intervals located just below the base of a large salt structure inducing variable illumination patterns. Figure 3 shows how depth-domain inversion helped reduce the illumination imprint, hindering amplitudes in the RTM image close to the salt boundary, leading to more balanced amplitudes, representative of the fluid content (brine and hydrocarbon) at the sand

intervals (Figure 3c) and to more reliable acoustic impedance (Figure 3d). The resolution of each interval is also considerably improved compared to the original RTM image.

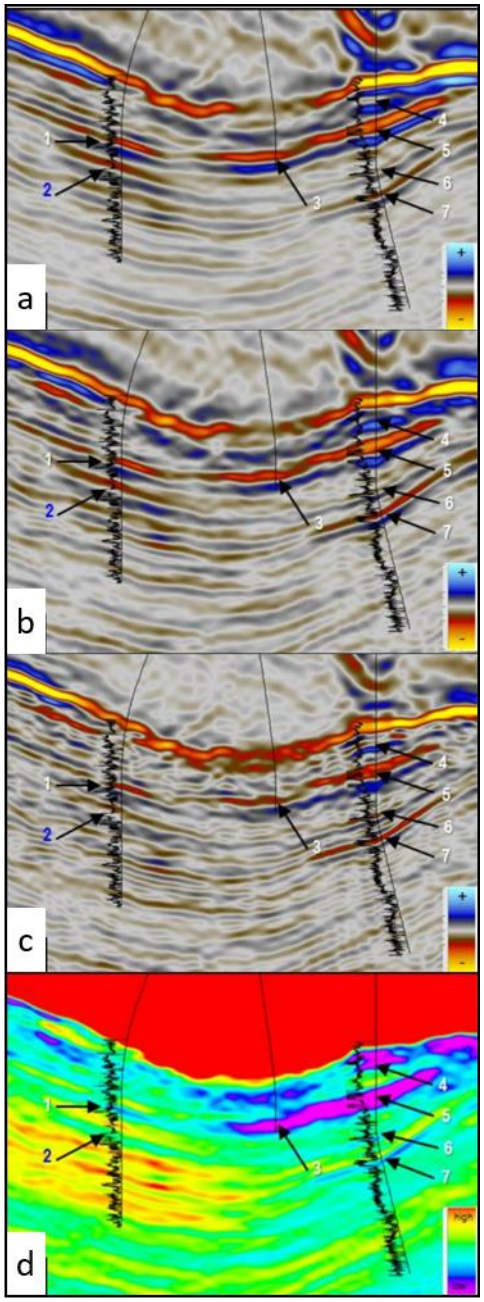

Figure 3 - *Mississippi Canyon (Gulf of Mexico) inversion example close to a salt structure (shown in red in (d)). Conventional RTM image (a), inverted reflectivities with (c) and without (b) PSF calibration, inverted acoustic impedance with PSF well calibration (d). Label 2 denotes brine sands whereas the six other labels indicate hydrocarbon sands. Acoustic impedance logs are superimposed. [From Leon et al., 2018]*

This example illustrates the importance of calibrating the PSFs at the well before inversion. By comparing the image to the result of convolving PSFs with the well reflectivity, matching filters were derived and applied to the PSFs. While the inverted reflectivity derived without calibration was already showing significant amplitude improvement (Figure 3b), higher resolution can be achieved after calibration (Figure 3d).

Inversion examples in the North Sea

Although the above examples illustrate the benefits of the approach in the presence of salt structures, depth-domain inversion has proven valuable in other complex geological environments. The following two examples are located in the North Sea.

In the first example from the Cook field (Leone et al., 2018b), illumination variations are induced by the interaction of a complex overburden and a limited narrow-azimuth acquisition geometry (Figure 4c) and generate large non-geological amplitude variations in the associated Kirchhoff depth migration image. Conventional time-domain inversion wrongly maps these variations into acoustic impedance variations (Figures 4a and 4d), whereas depth-domain inversion attenuates the illumination imprint and leads to more continuous and reliable acoustic impedance layers (Figures 4b and 4e). By appropriately handling the dip-dependent illumination and wavelet effects, it also leads to greater resolution improvement.

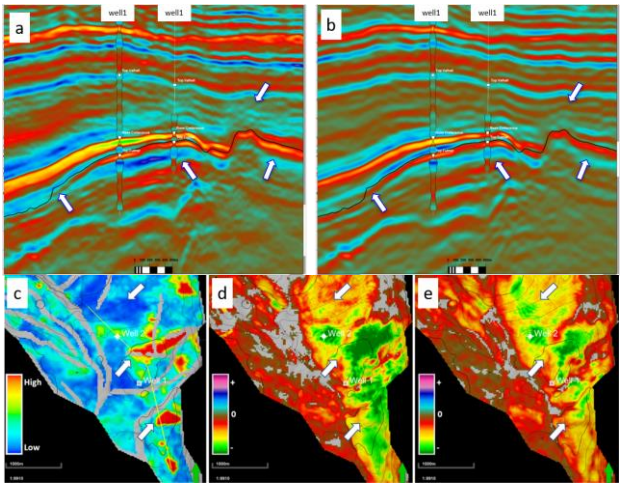

Figure 4 - *Cook field, North Sea example. Top row: acoustic impedance along an arbitrary line derived with conventional time-domain inversion (a) and depth-domain inversion (b). Bottom row: attribute maps for the target horizons denoted with a black line in Figures (a) and (b), hit-count maps (c), and minimum acoustic impedance extracted below the horizon from conventional time-domain inversion (d), and depth-domain inversion (e). A strong correlation is observed between the hit-count map and the acoustic impedance derived through conventional time-domain inversion. This illumination imprint is much reduced after depth-domain inversion. [From Leone et al., 2018b]*

Illumination maps are useful to get a better understanding of the potential impact of illumination variations on the seismic images and inversion results. While the map

shown in Figure 4c is a hit-count map derived through ray tracing, more insightful maps can be derived through PSF forward modelling. By convolving PSFs with an a priori reflectivity model built from interpreted horizons, synthetic images can be derived. These can be used to compute root-mean-square (RMS) amplitude maps along horizons to compare with those derived from the image. When strong correlation is observed, this indicates that the illumination imprint affects the image amplitudes and must be corrected for. An example can be found in Letki et al., 2015a. If no clear correlation exists, this may mean that either the migration velocity model used in the process does not capture the complexity creating the illumination effects visible in the image, or that the amplitude variations seen in the image are not related to illumination. In each case, PSF forward modelling can provide useful insights towards the nature of the amplitude variations observed in the image and/or the accuracy of the velocity model.

In the second example, from the Ivar Aasen field (Leone et al., 2018a), local illumination drops were encountered due to the presence of cemented sand injectites in the Oligocene, which are common in the North Sea. Provided that these local geological features can be properly modeled in the velocity field, depth-domain inversion can correct the local amplitude distortions created underneath (Figure 5).

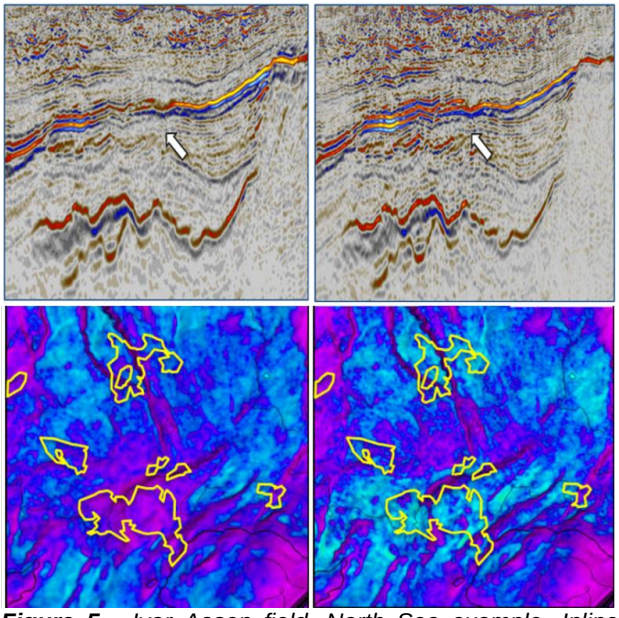

Figure 5 - *Ivar Aasen field, North Sea example. Inline section affected by a sand injectite body (top) and RMS amplitude maps along one target horizon (bottom) extracted from the Kirchhoff image (left) and from the reflectivity derived through depth-domain inversion (right). Yellow lines indicate the location of the overburden sand injectite bodies. In the amplitude maps, pink denotes low amplitude, blue denotes high amplitude. Depth-domain inversion greatly mitigates the sand injectite illumination imprint. [From Leone et al., 2018a]*

Prestack inversion examples

As reflectivity and elastic properties are related through the incident angle, prestack depth-domain inversion requires working with common-angle migrated gathers. Common source-direction gathers may also be inverted by converting source-direction angles into incident angles, on-the-fly, during the depth-domain inversion process (Du et al., 2016).

Yet, when necessary, the approach can be used to deblur common-offset gathers and derive deconvolved gathers compensated for illumination effects. In this case, the problem is parameterized in terms of reflectivity rather than elastic properties and regularization across offset can be used (cautiously) to stabilize the inversion at each offset. In the following synthetic example (Figure 6), the approach is used to deblur common-offset gathers and correct for illumination effects due to irregularities in the acquisition geometry. The illumination imprint, visible at short offsets, is reduced, potentially enabling more reliable elastic property estimation through subsequent conventional amplitude inversion. Another deblurring example with RTM surface-offset gathers can be found in the work of Dai et al. (2019). In both cases, a noticeable uplift in resolution is observed.

However, parameterizing the inversion in terms of elastic properties has several advantages and should probably be considered whenever common-angle gathers are available. Designing a reflectivity operator as well as appropriate earth property priors/constraints allows us to include more physics in the inversion problem. Moreover, deriving properties through one single inversion process should allow better noise handling. Both reflectivity images and earth properties are derived through the process, enabling enhanced structural and quantitative interpretation in one single step.

In the previous field data example from the Ivar Aasen field (Leone et al., 2018a), a prestack depth-domain inversion was conducted to estimate elastic properties (acoustic impedance and Vp/Vs) and perform lithology classification. Offset vector tiles were derived through Kirchhoff depth migration and converted into common-angle gathers using ray-tracing mapping. Common-angle PSFs were generated in a similar manner. Angle-dependent illumination and wavelet stretch effects present in each migrated gather were captured in the PSFs and accounted for during inversion. The illumination imprint beneath the sand injectites was much attenuated in the resulting prestack attributes as well as in the subsequent litho-classification volumes. Figure 7 shows a comparison of hydrocarbon probability maps derived from prestack conventional inversion and prestack depth-domain inversion. Depth-domain inversion noticeably improves the prediction underneath the sand injectites, facilitating the oil/water contact identification across the whole structure.

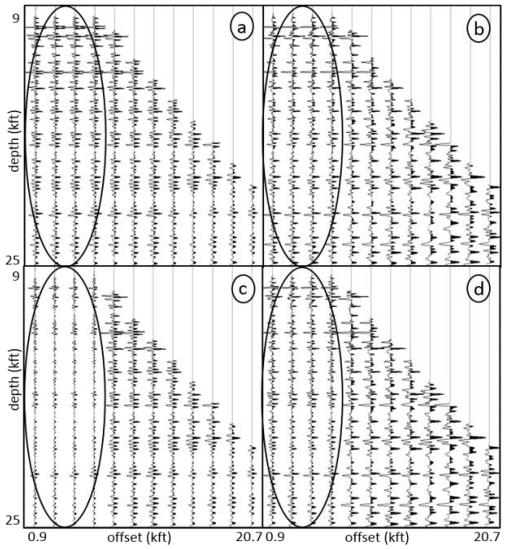

Figure 6 - *Sigsbee 2A synthetic example. Kirchhoff migrated offset gathers computed in a sediment area. Gathers before (left) and after (right) depth-domain inversion, using a regular acquisition geometry (top) and a decimated acquisition geometry where 70 % of the short offsets were randomly decimated (bottom). The amplitude dimming visible at short offset in Figure 6(c), caused by the restricted illumination, is significantly reduced after depth-domain inversion, leading to gathers that are quite similar to the inverted gathers based on the original geometry. [From Cavalca et al., 2016]*

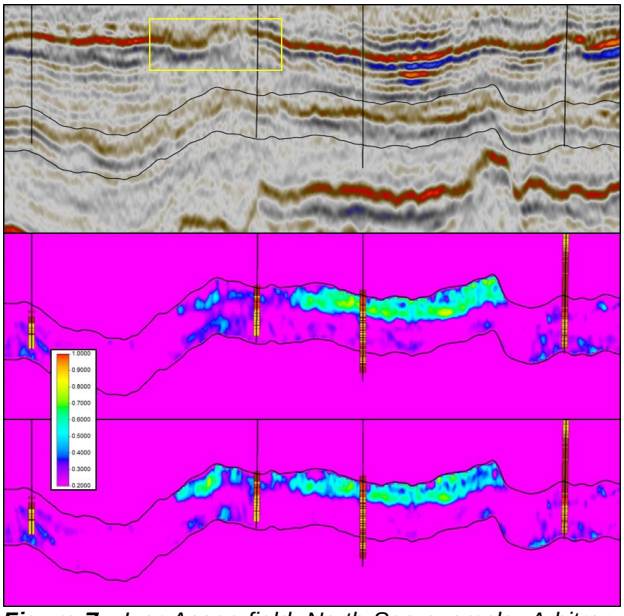

Figure 7 - *Ivar Aasen field, North Sea example. Arbitrary line through the Kirchhoff image (top). Hydrocarbon sand probability derived through conventional prestack time-domain inversion (middle) and prestack depth-domain inversion (bottom) in the window delimited by the two black lines. The probability derived through conventional inversion correlates well with the lithology except beneath the sand injectites. Depth-domain inversion significantly improves the prediction in this area. [From Leone et al., 2018a]*

4D inversion example

Thanks to its ability to capture and correct for illumination variations induced by different acquisition layouts, depth-domain inversion is naturally considered for 4D inversion of non-repeatable surveys. The approach is extended to poststack 4D simultaneous inversion. In this case, the inversion problem is parameterized in terms of baseline acoustic impedance and its perturbation. Constraints can be defined on the model perturbation if prior geological information is available.

In the following example, 4D depth-domain inversion was attempted on a complex synthetic inspired from the Thunder Horse field in the Gulf of Mexico, using data vintages generated with two radically different survey geometries: a narrow-azimuth streamer survey (baseline) and a wide-azimuth ocean-bottom nodes survey (monitor). In this example, illumination variations induced by the difference in acquisition layout were amplified by a complex overburden exhibiting a large salt structure shadowing the reservoirs. By capturing these variations in the PSFs, 3D depth-domain inversion mitigated the associated non-geological amplitude variations present in the RTM images of the two vintages (Figure 8) and 4D depth-domain inversion revealed interpretable 4D responses of the reservoirs that were previously hidden (Figure 9). While more investigations are required to fully understand the results from a quantitative perspective, this challenging example shows the potential of the approach to unlock time-lapse analysis from non-repeatable surveys.

Conclusions

Depth-domain inversion has proved to be an efficient method to handle illumination variations caused by complex geologies and limitations in acquisition geometries. It delivers higher-resolution reflectivity images more reflective of the underlying geology, as well as enhanced earth property estimates.

While poststack inversion is now used in many different geological environments, experience is being gained in prestack and 4D inversions. As for any least-squares migration approaches, the success of depth-domain inversion is dependent on the accuracy of the velocity model used in the process.

Acknowledgments

The authors thank Schlumberger for permission to publish this work as well as Claudio Leone, Leo Leon, Maria Shadrina, Laurence Letki, Britain Willingham, and the Schlumberger GeoSolution teams that processed the data shown in this abstract.

References

Caprioli, P.B.A., Du, X., Fletcher, R.P., and Vasconcelos, I. 2014. 3D source deghosting after imaging. 84th Annual

International Meeting, SEG, Expanded Abstracts, 4092-4096

Cavalca, M., Fletcher, R.P. and Du X. 2015. Q-compensation through depth domain inversion. 77th EAGE Conference & Exhibition, Extended Abstracts.

Cavalca, M, Fletcher, R.P. and Caprioli, P. 2016. Least-Squares Kirchhoff Depth Migration in the image domain. 78th EAGE Conference & Exhibition, Extended Abstracts.

Dai, W., Xu, Z., Cheng, X., Jiao, K. and Vigh, D. 2019. Image-domain Least-squares Migration for RTM Surface-offset Gathers. 81st EAGE Conference & Exhibition, Extended Abstracts.

Du, X., Fletcher, R.P. and Cavalca, M. 2016. Pre-stack depth domain inversion after reverse-time migration. 78th EAGE Conference & Exhibition, Extended Abstracts.

Fletcher, R.P., Archer, S., Nichols, D., and Mao, W. 2012. Inversion after depth imaging. 82nd Annual International Meeting, SEG, Expanded Abstracts.

Fletcher, R.P., Nichols D., Bloor R., and Coates R.T. 2016. Least-squares migration - Data domain versus image domain using point spread functions. The Leading Edge, 35, 157–162.

Fletcher, R.P., Cavalca, M. and Nichols D. 2018. Improving image-domain least-squares reverse-time migration close to high velocity contrasts. 80th EAGE Conference & Exhibition, Extended Abstracts.

Leon, L., Inyang, C., Hegazy, M., Hydal, S., Hargrove, K., Pasch, K. and Hollins, J. 2018. Least-squares migration in the image domain and depth-domain inversion: A Gulf of Mexico case study. 88th Annual International Meeting, SEG, Expanded Abstracts.

Leone, C., Osen, A., Cavalca, M., Fletcher, R.P. and Ferriday, M. 2018a. Improving Quantitative Interpretation beneath Sand Injectites: A North Sea Case Study. 80th EAGE Conference & Exhibition, Extended Abstracts.

Leone, C., Shadrina, M., Ramani, K., Cavalca, M. and Fletcher, R.P. 2018b. North Sea examples of Kirchhoff least-squares migration for quantitative interpretation. EAGE/SBGf Workshop on Least-Squares Migration.

Letki, L., Tang, J., Inyang, C., Du X. and Fletcher, R.P. 2015a. Depth domain inversion to improve the fidelity of subsalt imaging: a Gulf of Mexico case study, First Break, Vol 33, No 9, 81 – 85.

Letki, L., Darke, K., and Araujo Borges, Y. 2015b. A comparison between time domain and depth domain inversion to acoustic impedance. 85th Annual International Meeting, SEG, Expanded Abstracts.

Shadrina, M., Leone, C., Cavalca, M., Fletcher, R.P. and Gherasim, M. 2019. Revealing the time-lapse signal from non-repeatable vintages with 4D depth-domain inversion. 81st EAGE Conference & Exhibition, Extended Abstracts.

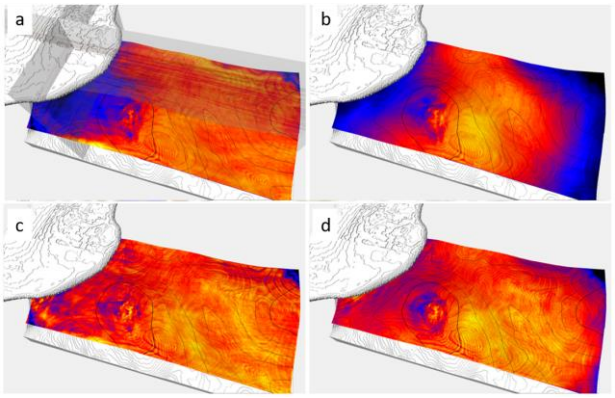

Figure 8 - *Thunder Horse synthetic example. RMS amplitude maps extracted along a target horizon with localized and small acoustic impedance changes: before (top) and after (bottom) depth-domain inversion for the narrow-azimuth baseline data (left) and the ocean-bottom node monitor data (right). Depth-domain inversion attenuates the illumination imprint of the salt structure for each of the acquisition systems, leading to more consistent amplitudes between the two vintages. [From Shadrina et al., 2019]*

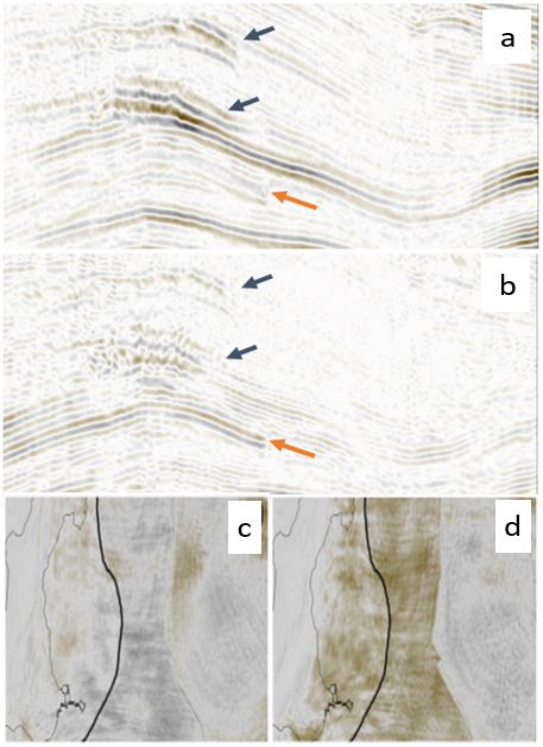

Figure 9 - *Thunder Horse synthetic example. Time-lapse response with no correction for illumination (a,c) and with 4D depth-domain inversion (b,d). The event denoted with the orange arrow indicates the reservoir associated with the predominant acoustic impedance change (5%). While it is hardly visible when illumination discrepancies are not accounted for (a), it is nicely revealed through 4D depth-domain inversion (b). The horizon slice through this event shown at the bottom confirms that the process enabled consistent recovery of the time-lapse response beneath the salt structure (denoted with the black line). [From Shadrina et al., 2019]*